Extension of a CUF-based vibroacoustic modal framework to fluid-loaded plates with simply-supported and free edges

CEAS Aeronautical Journal
https://doi.org/10.1007/s13272-026-00995-7

ORIGINAL PAPER

Extension of a CUF-based vibroacoustic modal framework to fluid-loaded plates with simply-supported and free edges

Dario Magliacano[1]

Received: 14 April 2026 / Revised: 27 June 2026 / Accepted: 2 July 2026

Abstract

This study extends a previously developed CUF-based frequency-domain framework for coupled vibroacoustic modal analysis to a rectangular fluid-loaded plate under simply-supported and free edge conditions. The physical system consists of an aluminum panel separating two surrounding air domains; the structural field is modeled by small-strain linear elasticity, and the acoustic field by linear, compressible acoustics. After enforcement of interface compatibility, the coupled displacement-pressure finite-element discretization yields a generalized eigenvalue problem. The spatial approximation combines cross-sectional Lagrange or Taylor expansions in the *x–z* plane with one-dimensional Lagrange interpolation along *y*, enabling systematic kinematic enrichment within the same CUF setting. The study focuses on the effect of non-clamped edges on the coupled spectrum, the comparison between Lagrange and Taylor cross-sectional expansions, and the MAC-based correlation between *in vacuo* and coupled modes. Validation against three-dimensional finite-element benchmarks is finally provided.

Keywords Vibroacoustics · Carrera unified formulation · Lagrange polynomials · Taylor expansion · Simply-supported boundary · Free edge · F–structure interaction · Modal assurance criterion · High-order finite elements

1 Introduction

Several studies in the relevant scientific literature have established the multiplicity of instability and vibroacoustic mechanisms that arise when elastic walls interact with internal or external flows, and have emphasized the influence of boundary conditions that depart from the fully clamped idealization and of material inhomogeneity on these mechanisms [1]. Building on this foundation, refined models generated within the Carrera Unified Formulation (CUF) now provide compact yet three-dimensionally consistent representations of structural kinematics, capturing warping, transverse shear, and through-thickness stretching effects without resorting to correction factors [2, 3]. In parallel, validation strategies have progressed from the classical Modal Assurance Criterion (MAC) towards energy-based correlation measures and unsupervised density-based clustering, which can reliably disentangle densely spaced fluid-loaded modes in the mid-frequency range [4–6]. Fluid–structure interaction in slender conduits and shell-like components remains a cornerstone topic for aerospace, marine, and energy applications.

1.1 Background and motivation

Predicting the dynamic behavior of slender structures that convey or contain fluids is crucial for a wide range of engineering systems, from lightweight aerospace tanks and piping networks to next-generation metamaterial waveguides [1, 7–9]. When the surrounding or enclosed fluid interacts with flexible walls, the resulting vibroacoustic response involves coupled structural and acoustic fields, so that both structural kinematics and the imposed edge constraints must be represented consistently. Classical first-order beam and shell theories disregard warping, shear, and thickness-stretching effects; consequently, they often fail to predict mode veering, frequency coalescence, and cross-modal energy exchange that are routinely observed in fluid–structure (FS) systems operating in the mid- to high-frequency

✉ Dario Magliacano
dario.magliacano@polito.it

[1] Department of Structural, Building, and Geotechnical Engineering, Politecnico di Torino, Corso Duca degli Abruzzi 24, 10129 Turin, Italy

Published online: 10 July 2026

range [10]. Refined theories generated within CUF have proved capable of overcoming these limitations by means of systematic high-order expansions along the cross-section, based initially on Taylor series and later extended to Lagrange, Legendre, and Chebyshev polynomials [11–13]. Nonetheless, most CUF-based vibroacoustic studies adopt clamped or periodic edges, whereas simply-supported and free boundaries, considered here as limiting non-clamped idealizations, are less frequently discussed. Recent investigations of coupled cylindrical shells have shown that switching from clamped to simply-supported edges can produce substantial frequency shifts due to the combined effects of reduced structural restraint and modified fluid–structure coupling [14]. Yet, a focused CUF-based assessment of these edge conditions for fluid-loaded plates remains lacking, despite the recent publication of the fully clamped reference framework [15].

A fluid-loaded eigenanalysis inherently generates displacement-pressure modes, in which structural and acoustic contributions may exchange dominance as frequency increases and as edge constraints are relaxed. In this setting, the central verification issue is not the availability of refined kinematics *per se*, but the objective tracking and pairing of modal vectors across (i) *in vacuo* versus coupled solutions and (ii) alternative cross-sectional representations (Taylor- versus Lagrange-based) under the same coupling and boundary scenario. Without a quantitative correlation metric, comparisons between different CUF hierarchies can be biased by mode veering and near-degeneracy, leading to ambiguous one-to-one correspondences. For this reason, MAC is employed here as a modal-correlation indicator to establish continuity between *in vacuo* and coupled solutions and to support comparisons between alternative cross-sectional expansions under identical coupling and boundary scenarios [4, 6, 16, 17].

1.2 State-of-the-art

Fluid-loaded plates and slender panels are canonical benchmarks for vibroacoustic modeling because they exhibit simultaneously (i) strong added-mass and radiation effects, (ii) a dense and rapidly varying modal content in the mid-frequency range, and (iii) a pronounced sensitivity to edge constraints. From a methodological standpoint, the coupled problem may be formulated in terms of structural displacement unknowns and an acoustic pressure field, yielding a nontrivial eigenvalue spectrum in which purely structural modes, purely acoustic cavity/field modes, and hybridized fluid–structure resonances can coexist. Classical structural acoustics references frame these aspects and discuss the practical consequences for sound radiation, transmission, and the prediction of response in engineering components.

From a numerical standpoint, vibroacoustic problems are most commonly tackled using coupled finite element (FE) formulations, in which the structural displacement and acoustic pressure fields are assembled into a single system via weak interface constraints. Within this class, displacement-pressure approaches offer a direct means of enforcing compatibility at the wetted surface. Still, they raise well-known issues related to stability and matrix symmetry, depending on the chosen variational setting and the adopted acoustic unknown. In bounded acoustic domains, symmetric alternatives based on potential variables have long been proposed to obtain energetically consistent coupled operators and continue to serve as a valuable reference for modal and harmonic analyses [18–20]. In realistic aerospace applications, however, the surrounding fluid domain is frequently unbounded or only partially confined; consequently, finite element discretizations are often complemented by boundary element couplings or by absorbing layers to emulate radiation conditions, with perfectly matched layers providing a robust attenuation strategy in the frequency domain [21, 22].

About numerical discretization, finite-element strategies for structural-acoustic interaction have long addressed stability and symmetry issues in the coupled operators. Early symmetric formulations and subsequent mixed displacement/pressure approaches clarified how spurious modes can arise when discrete spaces and boundary conditions are not consistently enforced [18, 19]. Complementary developments in computational acoustics consolidated the finite-element treatment of unbounded or truncated acoustic domains and provided a rigorous basis for absorbing or radiation-type boundary modeling [20]. In parallel, a broad family of reduced-order and wave-based techniques has been explored to mitigate the computational burden in the mid-frequency regime, where full three-dimensional meshes become rapidly prohibitive and where the structural and acoustic modal densities tend to increase markedly.

Beyond conventional FE/CUF formulations, vibration problems have also been addressed through reduced-order structural models, including discrete physical models, artificial neural network (ANN)-assisted predictors trained on high-fidelity data, dynamic-stiffness or transfer-matrix formulations, and semi-analytical beam models. Representative recent examples include the discrete model of tapered AFG beams by Moukhliss et al. [23], the ANN-based crack-detection framework of Moukhliss et al. [24, 25], the recent discrete physical model of non-uniform 2D-FGM beams, the dynamic-stiffness treatment of exponentially non-uniform beams with tip mass by Huang et al. [26], and the vibration/buckling analysis of rotating axially functionally graded nonuniform beams by Özdemir [27]. These contributions are valuable for structural vibration analysis, but they do not directly replace a coupled displacement-pressure formulation for fluid-loaded plates with explicitly discretized acoustic domains. For the present problem, the CUF-based FE route remains advantageous because it enables direct treatment of the structural and acoustic fields within the same weak-form setting and provides immediate access to coupled mode shapes and interface quantities.

A second, practically critical, aspect concerns boundary conditions. While simply-supported assumptions are attractive for analytical tractability and remain common in idealized benchmarks, actual engineering constraints are often intermediate between simply-supported, clamped, and free edges, and may vary along the perimeter due to joints, stiffeners, or mounting details. Such differences can alter both eigenfrequencies and mode families, and may substantially affect vibroacoustic coupling when structural and acoustic resonances approach each other [17]. Consequently, the state of the art increasingly emphasizes validation scenarios that include non-trivial edge conditions and that explicitly quantify the robustness of the predicted modal content across modeling choices.

Within this landscape, refined structural theories and high-order kinematics have been introduced to improve accuracy without resorting to uniformly fine three-dimensional discretizations. In this context, CUF has been used as a hierarchical framework to generate variable-kinematics finite elements, enabling systematic enrichment of cross-sectional fields while keeping the axial discretization comparatively compact [11, 12]. In particular, Cinefra et al. developed advanced CUF-based shell finite elements grounded in mixed variational statements, targeting laminated plates and shells where transverse shear and through-thickness effects are not negligible; these developments provide an enabling structural backbone when vibroacoustic coupling must be resolved with refined structural kinematics [28].

The Taylor expansion remains attractive for cross-sectional modeling within CUF because of its simplicity and the straightforward interpretation of each polynomial term as a thickness-wise derivative of the displacement field. Nevertheless, Arruda et al. showed that high-order Taylor models may suffer from ill-conditioning in sections, a drawback mitigated by recasting the expansion in terms of orthogonal Lagrange polynomials [29]. Carrera et al. further demonstrated that large cross-sectional deformations under geometrical nonlinearity require high-order expansions to obtain reliable results [30].

Finally, the credibility of vibroacoustic predictions in the mid-frequency range depends not only on the numerical solution strategy but also on the availability of verification indicators that can track mode families across modeling variants. The MAC remains a standard tool for correlating mode shapes, and it is often complemented by criteria for modal-density growth and energy localization in the mid-frequency domain [4, 16]. Recent work has also explored clustering-based and feature-driven strategies to improve the stability of mode matching and to support parametric studies in which boundary conditions or model order are varied [6]. In a closely related, yet distinct, direction, structured machine-learning and finite-element-informed surrogate pipelines have been proposed to extract predictive relationships from high-fidelity datasets for aerospace structures, including failure-related indicators in composite wing-box configurations with intralaminar damage, thereby contributing to data-assisted assessment workflows that can support monitoring or failure-related decision metrics when coupled with simulation-based evidence [31, 32].

Overall, the literature indicates that accurate vibroacoustic modal analysis of fluid-loaded plates requires, simultaneously, a stable coupled formulation, boundary-condition sensitivity, computationally efficient enrichment strategies, and verification metrics able to quantify mode correspondence under model changes. These needs motivate the present focus on cross-sectional expansion choices and edge constraints within a unified and verifiable modeling framework.

1.3 Scope and contributions of the present study

The present work does not introduce a new coupled formalism from scratch. Rather, it extends the CUF-based vibroacoustic modal framework previously introduced in [15] to a new class of plate edge conditions. The specific contributions lie in the assessment of simply-supported and free boundaries, the comparison between Lagrange and Taylor cross-sectional expansions under the same fluid–structure setting, and the use of MAC to establish modal correspondence between *in vacuo* and coupled solutions.

From this perspective, CUF provides a hierarchical setting in which three-dimensional kinematics is represented by an *a priori* separable expansion of the field variables. By increasing either the degree or the family of the cross-sectional polynomials, the approximation can be enriched without changing the general structure of the governing FE operators. In this way, the formulation preserves substantially fewer unknowns than a full three-dimensional discretization for comparable accuracy, while remaining fully compatible with standard weak forms for structural-acoustic interaction. The remainder of the paper is organized as follows. Section 2 summarizes the governing equations and the CUF-based (FE) implementation. Section 3 delineates the model's geometric configuration, material properties, and boundary conditions employed to validate the proposed coupled vibroacoustic formulation. Section 4 validates the adopted formulation against three-dimensional commercial codes. Section 5 presents a detailed investigation of the influence of boundary conditions and Taylor order on the modal characteristics. Finally, Sect. 6 draws the main conclusions and outlines future research directions.

2 Methodological framework

The methodological framework adopted in this work is a coupled finite element formulation implemented in CUF. The structural displacement field and the acoustic pressure field are approximated through Lagrange or Taylor expansions over the cross-section, while one-dimensional Lagrange interpolation is used along the remaining coordinate. The resulting approximation supports systematic kinematic enrichment within a common FE setting and, upon fluid–structure coupling, yields a generalized eigenvalue problem.

The uncoupled structural and acoustic symmetric eigenproblems were solved by sparse shift-invert Lanczos. The coupled problem was treated in its assembled non-symmetric generalized form by a shift-invert Arnoldi procedure after sparse LU factorization of the shifted pencil. Convergence was monitored on the relative residual norms of the computed Ritz pairs.

2.1 Kinematic assumptions

Although the physical domain is a rectangular plate, the adopted CUF representation is factorized: the coordinates (x, z) are handled through cross-sectional expansions, whereas the remaining coordinate y is discretized by one-dimensional finite elements. The notation therefore resembles variable-kinematics beam formulations, but the geometry, constitutive model, and coupling operators remain three-dimensional and are specialized here to a plate-like domain. Within CUF, the three displacement components may be collected in the vector

$$\mathrm{u}(x,y,z,\omega)=\begin{bmatrix}u(x,y,z,\omega)\\ v(x,y,z,\omega)\\ w(x,y,z,\omega)\end{bmatrix}. \tag{1}$$

Here ω denotes the angular frequency and a time-harmonic dependence $\mathrm{e}^{\mathrm{i}\omega t}$ is assumed; u, v, and w are the displacement components along the x-, y-, and z-axes, respectively. Note that $w(\cdot)$ will later denote Gauss-Legendre weights in numerical quadrature, whereas w in Eq. (12) will denote a (virtual) test function. The vector $\mathrm{u}(x,y,z,\omega)$ is expanded along the coordinates $\{x,z\}$ as

$$\mathrm{u}(x,y,z)=F_\tau(x,z)\,\mathrm{u}_\tau(y),\quad \tau=1,2,\ldots,M_u, \tag{2}$$

in which F_τ represents the retained cross-sectional expansion functions, u_τ indicates the generalized displacement vector depending on the y coordinate, M_u is the number of retained displacement expansion terms, and the repeated index τ denotes summation. The through-length variation is captured through one-dimensional shape functions,

$$\mathrm{u}_\tau(y)=N_i(y)\,\mathrm{q}_{\tau i},\quad i=1,2,\ldots,n_{\mathrm{el}}, \tag{3}$$

in which N_i are the ith shape functions, $\mathrm{q}_{\tau i}$ represents the unknown nodal variables, n_{el} is the number of nodes per element and i indicates summation. The same hierarchical expansion is employed for the acoustic pressure,

$$p(x,y,z)=G_\tau(x,z)\,p_\tau(y),\quad \tau=1,2,\ldots,M_p, \tag{4}$$

where $G_\tau(x,z)$ are the retained cross-sectional pressure functions and $p_\tau(y)$ are the generalized pressure amplitudes along the y-axis, so that structural and fluid fields share compatible interface discretizations. Interpolation in the cross-section (x, z) employs quadrilateral Lagrange elements: LE4 (bilinear, degree 1), LE9 (biquadratic, degree 2), and LE16 (bicubic, degree 3). The through-thickness coordinate y is approximated by a one-dimensional B3 Lagrange polynomial (quadratic, degree 2). For the Lagrange-based models, F_τ and G_τ are standard tensor-product quadrilateral interpolation functions over the parent cross-section. For the Taylor-based models, the retained basis consists of the complete monomials $x^a z^b$ of total degree $a+b\le p$, so that the number of retained terms is $M=(p+1)(p+2)/2$. Numerical integration is carried out by Gauss-Legendre quadrature using (2×2) points for LE4, (3×3) for LE9, (4×4) for LE16 in the cross-section, and a 3-point rule along y. The shorthand adopted throughout the paper follows the convention LEnBm, where LEn identifies the Lagrange cross-sectional interpolation with n nodes in the (x, z) plane, while Bm identifies the one-dimensional Lagrange interpolation adopted along y. Thus, LE4B3, LE9B3, and LE16B3 differ in the polynomial order and number of cross-sectional interpolation nodes, not in the underlying physical model. Similarly, TE p B3 denotes a total-degree Taylor expansion of order p over the cross-section combined with the same B3 interpolation along y. This configuration exactly integrates products of shape functions and their derivatives up to the corresponding degrees. Figure 1 provides a schematic overview of the coupled domains and the locations of the mixed boundary conditions.

2.2 Variational formulation and element matrices

Application of the principle of virtual work yields the elemental stiffness and mass matrices for the structure,

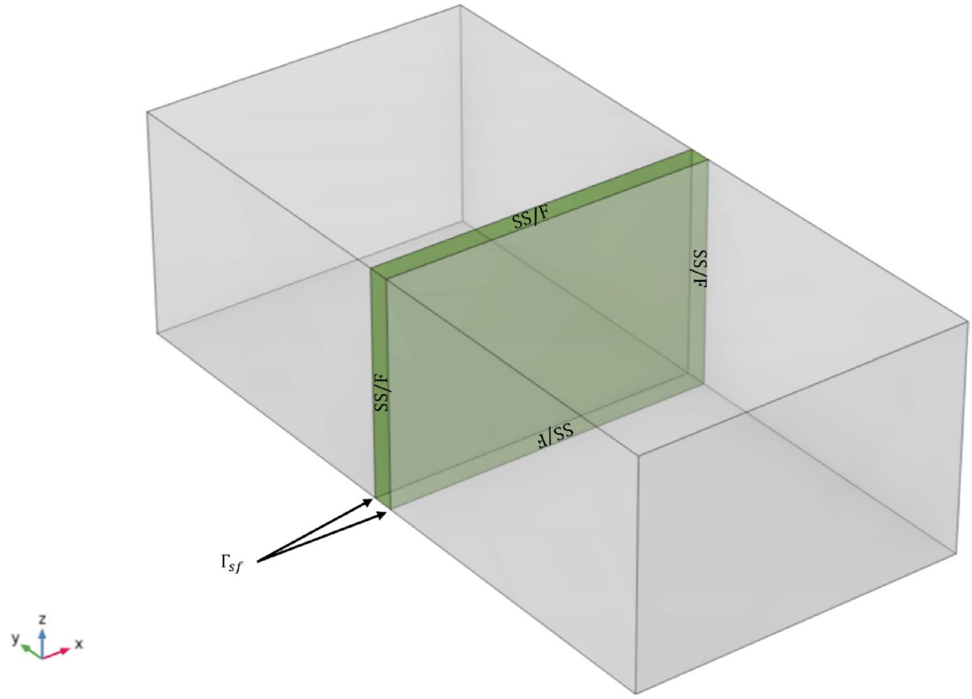

Fig. 1 Schematic of the coupled domains and imposed boundary conditions. The aluminum plate is shown in green, the surrounding air layers in gray, the fluid–structure interfaces by Γ_{sf}, and the truncated outer acoustic surfaces by $p = 0$. The lateral structural edges are alternately treated as simply-supported (SS) or free (F), depending on the benchmark case

$$\mathrm{K}^e_{ss} = \int_{-1}^{1}\int_{-1}^{1}\int_{-1}^{1} \mathrm{B}^T\mathrm{D}\mathrm{B}\,|J_{xz}(\xi,\eta)|\,|J_y(\zeta)|\,\mathrm{d}\xi\,\mathrm{d}\eta\,\mathrm{d}\zeta, \tag{5}$$

$$\mathrm{M}^e_{ss} = \int_{-1}^{1}\int_{-1}^{1}\int_{-1}^{1} \rho\,\mathrm{N}^T\mathrm{N}\,|J_{xz}(\xi,\eta)|\,|J_y(\zeta)|\,\mathrm{d}\xi\,\mathrm{d}\eta\,\mathrm{d}\zeta, \tag{6}$$

$$\mathrm{K}^e_{ff} = \int_{-1}^{1}\int_{-1}^{1}\int_{-1}^{1} \kappa\,(\nabla\mathrm{N}_p)^T(\nabla\mathrm{N}_p)\,|J_{xz}(\xi,\eta)|\,|J_y(\zeta)|\,\mathrm{d}\xi\,\mathrm{d}\eta\,\mathrm{d}\zeta, \tag{7}$$

$$\mathrm{M}^e_{ff} = \int_{-1}^{1}\int_{-1}^{1}\int_{-1}^{1} \rho_f\,\mathrm{N}_p^T\mathrm{N}_p\,|J_{xz}(\xi,\eta)|\,|J_y(\zeta)|\,\mathrm{d}\xi\,\mathrm{d}\eta\,\mathrm{d}\zeta, \tag{8}$$

where the subscripts *ss* and *ff* denote structural-structural and fluid-fluid matrix blocks, respectively, and |*J*| is the determinant of the complete element mapping. The coefficient $\kappa = \rho_f c_f^2$ is the bulk modulus of the acoustic medium, with ρ_f and c_f being the fluid density and sound speed. The Jacobian is factorized as

$$|J(\xi,\eta,\zeta)| = |J_{xz}(\xi,\eta)||J_y(\zeta)|, \quad |J_{xz}(\xi,\eta) \\ | = \det\begin{bmatrix} \frac{\partial x}{\partial \xi} & \text{amp;}\,\frac{\partial x}{\partial \eta} \\ \frac{\partial z}{\partial \xi} & \text{amp;}\,\frac{\partial z}{\partial \eta} \end{bmatrix}, \quad |J_y(\zeta)| = \frac{\partial y}{\partial \zeta}. \tag{9}$$

In Eq. (9), ξ and η are the natural coordinates of the two-dimensional parent element in the cross-section (*x*, *z*), whereas ζ is the natural coordinate of the one-dimensional interpolation along *y*. Therefore, $|J_{xz}(\xi,\eta)|$ is the Jacobian determinant of the cross-sectional mapping and $|J_y(\zeta)|$ is the one-dimensional Jacobian associated with the *y*-direction.

In the actual numerical implementation, the integrals in Eqs. (5)–(8) are evaluated by Gauss-Legendre quadrature using the rules stated in Sect. 2.1. The matrix B is the strain–displacement matrix associated with the adopted CUF kinematics, D is the linear elastic constitutive matrix, N collects the structural displacement shape functions, and N_p collects the acoustic pressure shape functions. The symbols ρ and ρ_f denote the solid and fluid mass densities, respectively. Assembly of the structural matrices leads to the *in vacuo* eigenproblem

$$\mathrm{K}_{ss}\,\hat{\mathrm{u}} - \omega^2\mathrm{M}_{ss}\,\hat{\mathrm{u}} = 0, \tag{10}$$

whereas in the acoustic domain, the Helmholtz equation,

$$\nabla^2\tilde{p} + k^2\tilde{p} = 0. \tag{11}$$

In Eq. (11), $\tilde{p}$ is the complex-valued acoustic pressure amplitude and *k* is the acoustic wavenumber, defined as $k = \omega/c_f$, giving rise to the weak form

$$\int_{\Omega_f} \nabla w\cdot\nabla\tilde{p}\,\mathrm{d}\Omega_f - k^2\int_{\Omega_f} w\,\tilde{p}\,\mathrm{d}\Omega_f = \int_{\Gamma_q} w\,\bar{q}\,\mathrm{d}\Gamma_q. \tag{12}$$

In Eq. (12), Ω_f denotes the fluid (acoustic) domain and $\Gamma_q \subset \partial\Omega_f$ is the portion of its boundary where a Neumann-type datum $\bar{q}$ (prescribed normal flux/velocity-related quantity) is imposed; *w* is an admissible test function (virtual pressure field). The corresponding discrete problem is

$$\mathrm{K}_{ff}\,\hat{\mathrm{p}} - \omega^2 \mathrm{M}_{ff}\,\hat{\mathrm{p}} = 0. \tag{13}$$

In Eqs. (10) and (13), $\hat{\mathrm{u}}$ and $\hat{\mathrm{p}}$ denote the structural and acoustic eigenvectors (mode-shape amplitudes), and $\omega = 2\pi f$ is the circular eigenfrequency.

2.3 Fluid–structure coupling

Fluid–structure coupling is central, capturing interaction between acoustic and structural fields. In the frequency domain, this is enforced via interface conditions (continuity of normal acceleration and equilibrium of normal tractions) that link motion to the pressure gradient. These read:

$$\frac{\partial p}{\partial n} = -\rho_f \omega^2 n \cdot \mathrm{u} \quad \text{on } \Gamma_{sf}, \quad \sigma n = -pn \quad \text{on } \Gamma_{sf}, \tag{14}$$

where u is the structural displacement, *p* the acoustic pressure, *n* the unit normal (fluid→structure), ρ_f the fluid density, and Γ_{sf} the interface. Their weak imposition leads to the non-symmetric coupling operators used herein. Here $\boldsymbol{\sigma}$ is the Cauchy stress tensor in the solid and *n* (equivalently $\boldsymbol{n}$ in the following) denotes the unit outward normal at the interface. In Eqs. (15), (16), N_u and N_p are, respectively, the structural and acoustic interpolation functions on Γ_{sf} ; n_e is the number of interface nodes per element, while M_u and M_p denote the numbers of retained CUF expansion terms for the displacement and pressure fields. The operator $\mathrm{B}_\sigma^{i\tau}$ represents the discrete mapping from the generalized structural degrees of freedom associated with node *i* and expansion index τ to the interface traction contribution entering the pressure-to-traction coupling integral. The above expressions are classical in displacement-pressure fluid–structure interaction (FSI) formulations for structural acoustics [18]. In the assembled system $\mathrm{K} + \omega^2\mathrm{M}$, the coupling matrices arise from the interface integrals. With standard finite-element shape functions N_u (structure) and N_p (fluid), and normal $\boldsymbol{n}$, one obtains schematically

$$\mathrm{K}_{sf} = \sum_{i=1}^{n_e}\sum_{j=1}^{n_e}\sum_{\tau=1}^{M_u}\sum_{\sigma=1}^{M_p} \mathrm{K}_{sf}^{i\tau,j\sigma}, \quad \mathrm{K}_{sf}^{i\tau,j\sigma} = \int_{\Gamma_{sf}} \left(\mathrm{B}_\sigma^{i\tau}\right)^{\top} \mathrm{n}\, N_p^{j\sigma}\, \mathrm{d}\Gamma, \tag{15}$$

$$\mathrm{M}_{fs} = \sum_{j=1}^{n_e}\sum_{i=1}^{n_e}\sum_{\sigma=1}^{M_p}\sum_{\tau=1}^{M_u} \mathrm{M}_{fs}^{j\sigma,i\tau}, \quad \mathrm{M}_{fs}^{j\sigma,i\tau} = \int_{\Gamma_{sf}} N_p^{j\sigma} \rho_f\, \mathrm{n}\mathrm{n}^{\top}\, \mathrm{N}_u^{i\tau}\, \mathrm{d}\Gamma. \tag{16}$$

Because the integrations in Eqs. (15), (16) are restricted to Γ_{sf}, the resulting coupling blocks are sparse at the global level: only structural and acoustic degrees of freedom belonging to the wetted interface contribute to the off-diagonal operators. They are not diagonal matrices, since each interface element couples all locally supported structural and pressure interpolation functions. They are also not globally full, because degrees of freedom not connected to the fluid–structure boundary produce identically zero entries in these coupling blocks. Here K_{sf} maps pressure to structural tractions, whereas M_{fs} maps structural normal acceleration to acoustic pressure. The two off-diagonal contributions therefore belong to different operators. Accordingly, the coupled generalized eigenproblem is written as

$$\left(\begin{bmatrix} \mathrm{K}_{ss} & \mathrm{K}_{sf} \\ 0 & \mathrm{K}_{ff} \end{bmatrix} - \omega^2 \begin{bmatrix} \mathrm{M}_{ss} & 0 \\ \mathrm{M}_{fs} & \mathrm{M}_{ff} \end{bmatrix} \right) \begin{bmatrix} \hat{\mathrm{u}} \\ \hat{\mathrm{p}} \end{bmatrix} = 0. \tag{17}$$

Equation (17) is non-symmetric because the upper-right and lower-left coupling blocks belong to different operators and are not transpose counterparts of each other.

2.4 Modal assurance criterion

Correlation between numerical eigenvectors computed among *in vacuo* and FS coupled models is quantified through the MAC,

$$\mathrm{MAC}_{ij} = \frac{\left|\boldsymbol{\phi}_i^{\mathrm{T}} \boldsymbol{\phi}_j\right|^2}{\left(\boldsymbol{\phi}_i^{\mathrm{T}} \boldsymbol{\phi}_i\right)\left(\boldsymbol{\phi}_j^{\mathrm{T}} \boldsymbol{\phi}_j\right)}, \tag{18}$$

In Eq. (18), $\boldsymbol{\phi}_i$ and $\boldsymbol{\phi}_j$ denote the eigenvectors (mode shapes) extracted from the two models being compared, consistently sampled over the same set of degrees of freedom. The subscripts *i* and *j* are modal indices: in the present application, *i* runs over the selected *in vacuo* modes, whereas *j* runs over the coupled fluid–structure modes. They are therefore not spatial, nodal, or expansion indices. The superscript T indicates transpose (for real-valued modes as considered herein). The MAC assumes values in [0, 1], with unity denoting perfect agreement [16].

3 Model description

The physical system examined is a flat, rectangular aluminum plate that seals a cavity subdivided into two acoustically coupled air volumes, as illustrated in Fig. 1. The structural region under investigation is an aluminum rectangular plate whose breadth and height lie in the $x - z$ plane, whereas its thickness develops along the *y* direction. Its planform dimensions are $L_x = 15\,\mathrm{cm}$, $L_y = 1\,\mathrm{cm}$, and $L_z = 10\,\mathrm{cm}$. For convergence checks, all perimeter edges located at $x = 0$, $x = L_x$, $z = 0$, and $z = L_z$ were temporarily idealized as fully clamped, a boundary configuration routinely adopted to benchmark flexural stiffness in fluid-loaded panel studies [33]. In the present work, convergence is declared when successive refinements change the target eigenfrequencies by less than 1%, consistently with the criterion adopted in the COMSOL validation reported in Sect. 4 and with standard verification practice [34, 35].

The acoustic domain consists of two truncated air layers, contiguous with the plate faces at $y = 0$ and $y = L_y$, each reproducing the structure's in-plane footprint and ensuring kinematic compatibility across the interface. The fluid is modeled as a linear, compressible, and inviscid acoustic medium. In the present modal benchmarks, the outer faces of the truncated layers are assigned homogeneous Dirichlet conditions, $p = 0$, so that the model represents a finite pressure-release cavity surrounding the panel rather than an exterior-radiation problem. The thickness of each air layer is chosen as a geometric truncation parameter large enough to separate the plate from the outer pressure-release surface; exterior-radiation treatments based on impedance conditions or perfectly matched layers are not considered here. In interior acoustics, a pressure-release (Dirichlet) boundary reflects with phase inversion [20] and is used here to define a finite interior cavity surrounding the structure. For exterior radiation or open-domain emulation, standard treatments use impedance (Robin) conditions or perfectly matched layers (PMLs) [20]. The present study treats interior eigenmodes; exterior-radiation modeling is deferred.

The choice of a single metallic panel, rather than a shell or a multi-layer composite, isolates the influence of boundary constraints and cross-sectional kinematics on the fluid–structure interaction problem and provides a direct benchmark for the adopted high-order formulation. The lateral structural boundaries are alternately treated as free and as a simply-supported case. In the latter, the implemented three-dimensional constraint sets $u_x = u_z = 0$ along the lateral edges, while the remaining kinematic components are left free; this condition is used here as the adopted non-clamped support idealization within the present CUF discretization, and should not be read as a direct restatement of the classical Kirchhoff-Love simply-supported condition. In the free case, no structural displacement constraints are applied. The cross-sectional displacement and pressure fields are approximated by bilinear, biquadratic, or bicubic Lagrange polynomials, or, for the uncoupled domains, by total-degree Taylor polynomials up to fifth order; the attendant increase in the number of generalized coordinates is offset by the hierarchical nature of the expansion, which allows a systematic convergence study in Sect. 5. The surrounding acoustic domain is discretized with elements that share the same Gauss integration points as those on the structural side, thereby ensuring a conforming fluid–structure interface. Homogeneous pressure-release conditions are enforced on the truncated outer fluid surfaces. The acoustic mesh is built so that the shortest wavelength in the frequency range of interest (corresponding to the quarter-wave resonance of the deeper cavity) remains resolved by at least six linear elements (or an equivalent number of high-order ones), in line with the recommendations of Biedermann et al. [4]. Coupling matrices are assembled according to Eqs. (15) and (16), after mapping the normal traction exerted by the plate onto the fluid pressure field and vice versa through consistent shape-function interpolation [2].

Table 1 Material properties of the structure (aluminum) and the fluid (air)

Property	Aluminum	Air
Young's modulus, E	70 GPa	–
Poisson's ratio, ν	0.33	–
Density, ρ	2700 $\frac{\mathrm{kg}}{\mathrm{m}^3}$	1.2 $\frac{\mathrm{kg}}{\mathrm{m}^3}$
Speed of sound, c	–	343 $\frac{\mathrm{m}}{\mathrm{s}}$

Table 1 collects the mechanical and acoustical constants adopted throughout the study. The aluminum properties coincide with those previously used by Magliacano et al. [15]; the air density and speed of sound are evaluated at 20 °C, by ISO 9613-1, and kept constant because the Mach number associated with plate vibrations never exceeds 10^{-3}.

4 Formulation validation

The predictive capabilities of CUF for fluid-loaded waveguides have already been established in the literature; nonetheless, a tailored benchmark is presented here to substantiate the present implementation against a full three-dimensional finite element model in COMSOL Multiphysics 6.2. For the displacement field, COMSOL uses quadratic serendipity shape functions, meaning 20-node serendipity hexahedra with quadratic interpolation along the element edges and without face- or interior nodes; instead, for the pressure field, quadratic Lagrangian shape functions are used. This structural choice is relevant from the viewpoint of degrees of freedom, since a full quadratic hexahedral Lagrange element would contain additional face and internal nodes, whereas the serendipity element preserves quadratic boundary interpolation with a smaller number of element-level unknowns. To ensure a true like-for-like comparison, the structural and acoustic material constants and boundary conditions adopted in Sect. 2 and 3 are reproduced exactly in the reference model. Owing to the rectangular geometry of both the plate and the acoustic layers, the reference FE mesh is generated through a structured mapped/swept procedure, leading to regular hexahedral elements with matching topology across the fluid–structure interface. The mesh is refined by increasing the number of elements while preserving the same mapped distribution, so that changes in the computed eigenfrequencies are attributable to resolution rather than to changes in mesh topology. Mesh refinement is driven by the relative variation of consecutive eigenfrequencies, quantified through the convergence index

$$\text{error}\,[\%] = \frac{\mathrm{m_{i\,+\,1}} - \mathrm{m_i}}{\mathrm{m_i}} \tag{19}$$

where

- m_{i+1} an eigenfrequency obtained with a finer mesh;
- m_i is an eigenfrequency obtained with a coarser mesh.

All tabulated frequencies are rounded to the nearest hertz. Following the well-established criteria [11, 36], an error threshold of 1% is deemed sufficient for modal analyses of lightly damped aluminum panels. Under this requirement, the COMSOL model converges with 5565 structural DoFs, 84,987 total (structural + fluid) DoFs, and 150 cross-section elements; the CUF LE4B3 model converges with 22,509 structural DoFs, 177,571 total DoFs, and 2400 cross-section elements; the CUF LE9B3 model converges with 5859 structural DoFs, 46,221 total DoFs, and 150 cross-section elements; the CUF LE16B3 model converges with 3600 structural DoFs, 28,400 total DoFs, and 40 cross-section elements. The resulting eigenfrequencies for the simply-supported configuration are summarized in Table 2; a second benchmark considers the plate with free edges. Table 3 lists the corresponding frequencies. CUF solutions deviate from the three-dimensional benchmark by less than 0.6% over the first ten elastic-acoustic modes, thereby corroborating the accuracy of the adopted high-order factorized formulation.

To assess the influence of cross-sectional kinematics, Lagrange-based (LE) and Taylor-based (TE) cross-sections are compared for the free-edge case. These data, obtained for an isolated unconstrained structure (Table 4) and an isolated rigid fluid (Table 5), whose material and geometrical properties are the same as those reported in Sect. 3. Although the Taylor expansion employs far fewer DoFs (54 for TE2B3 against more than 22,000 for LE4B3), the isolated structural benchmark shows a progressive, but not uniform, convergence with increasing Taylor order. The average frequency deviation decreases from 59.65% for TE2B3 to 15.88% for TE3B3, 5.71% for TE4B3, and 2.17% for TE5B3. Therefore, the Taylor basis should be regarded here as a compact reduced kinematic representation whose reliability becomes acceptable only at sufficiently high order.

The isolated rigid-fluid benchmark of Table 5 can also be checked against the closed-form eigenfrequencies of a rectangular rigid-walled acoustic cavity. This analytical check is deliberately restricted to one isolated fluid layer and is not intended to represent the complete two-layer coupled plate-fluid system. For a cavity with dimensions L_x, L_y^f, and L_z, the Neumann spectrum is

$$f_{lmn}^{\text{an}} = \frac{c_f}{2}\sqrt{\left(\frac{l}{L_x}\right)^2 + \left(\frac{m}{L_y^f}\right)^2 + \left(\frac{n}{L_z}\right)^2}, \quad l, m, n = 0, 1, 2, \ldots, \tag{20}$$

where l, m, and n are the acoustic modal indices along x, y, and z, respectively, and the triplet $(l, m, n) = (0, 0, 0)$ corresponds to the constant-pressure zero mode. In the present isolated-fluid check, $L_x = 0.15\,\text{m}$, $L_y^f = 0.15\,\text{m}$, $L_z = 0.10\,\text{m}$, and $c_f = 343\,\text{m/s}$. The analytical frequencies reported in Table 5 are the first ten values of Eq. (20), sorted in ascending order and rounded to the nearest hertz. This comparison provides an additional verification of the isolated acoustic subproblem, complementing but not replacing the coupled fluid–structure benchmark against COMSOL [20, 37].

In summary, the CUF-based factorized formulation reproduces the three-dimensional FE reference solutions with

Table 2 Comparison of eigenfrequencies between COMSOL and CUF, concerning the coupled (fluid–structure) model. Aluminum material, simply-supported structural, and pressure-release fluid boundary conditions. The average frequency shifts relative to COMSOL Multiphysics 6.2 are 0.18%, − 0.03%, and − 0.02%, respectively

Approach	COMSOL	LE4B3	LE9B3	LE16B3
Degrees of freedom	84,987	177,571	46,221	28,400
Eigenfrequencies [Hz]	0	0	0	0
	1078	1091	1079	1078
	2140	2138	2138	2139
	2141	2139	2139	2139
	2403	2432	2406	2407
	2683	2680	2681	2681
	2683	2682	2682	2682
	2917	2911	2915	2915
	2917	2916	2916	2918
	3335	3329	3333	3333

Table 3 Comparison of eigenfrequencies between COMSOL and CUF, concerning the coupled (fluid–structure) model

Approach	COMSOL	LE4B3	LE9B3	LE16B3
Degrees of freedom	84,987	177,571	46,221	28,400
Eigenfrequencies [Hz]	0	0	0	0
	0	0	0	0
	0	0	0	0
	0	0	0	0
	0	0	0	0
	0	0	0	0
	2073	2080	2079	2079
	2140	2139	2138	2134
	2140	2154	2140	2139
	2296	2329	2298	2301

Aluminum material, free structural, and pressure-release fluid boundary conditions. The average frequency shifts relative to COMSOL Multiphysics 6.2 are 0.59%, 0.06%, and 0.03%, respectively

Table 4 Comparison of eigenfrequencies between COMSOL and CUF (with cross-section Taylor expansion)

Approach	COMSOL	LE4B3	LE9B3	LE16B3	TE2B3	TE3B3	TE4B3	TE5B3
Degrees of freedom	21,015	22,509	5859	3600	54	90	135	189
Eigenfrequencies [Hz]	0	0	0	0	0	0	0	0
	0	0	0	0	0	0	0	0
	0	0	0	0	0	0	0	0
	0	0	0	0	0	0	0	0
	0	0	0	0	0	0	0	0
	0	0	0	0	0	0	0	0
	2071	2081	2081	2080	2263	2229	2145	2117
	2296	2328	2298	2298	2708	2678	2323	2317
	4713	4756	4742	4741	6483	5647	5359	4932
	5288	5359	5300	5298	14,478	6314	5518	5336

Aluminum material, free structural boundary conditions. The average frequency shifts relative to COMSOL Multiphysics 6.2 are 1.04%, 0.36%, 0.34%, 59.65%, 15.88%, 5.71%, and 2.17%, respectively

Table 5 Comparison of eigenfrequencies between the analytical rigid-cavity solution, COMSOL, and CUF (with cross-section Taylor expansion)

Approach	Analytical	COMSOL	LE4B3	LE9B3	LE16B3	TE2B3	TE3B3	TE4B3	TE5B3
Degrees of freedom	–	13,671	77,351	20,181	12,400	186	310	465	651
Eigenfrequencies [Hz]	0	0	0	0	0	0	0	0	0
	1143	1144	1143	1143	1143	1143	1143	1143	1143
	1143	1144	1143	1143	1143	1261	1144	1144	1143
	1617	1618	1617	1617	1617	1702	1617	1617	1617
	1715	1716	1715	1715	1715	1891	1715	1715	1715
	2061	2062	2062	2061	2061	2210	2062	2062	2061
	2061	2062	2062	2061	2061	2273	2273	2065	2065
	2287	2288	2287	2287	2287	2287	2287	2287	2287
	2287	2288	2288	2287	2287	2544	2544	2295	2295
	2357	2359	2357	2357	2357	2611	2557	2360	2360

Air material, rigid fluid boundary conditions. The average frequency shifts relative to COMSOL Multiphysics 6.2 are − 0.04%, − 0.06%, − 0.06%, 7.19%, 3.28%, 0.02%, and 0.01%, respectively

sub-percent discrepancies when Lagrange polynomials of moderate order are employed. The Taylor hierarchy exhibits greater sensitivity to truncation order: the lowest-order Taylor models are insufficient for the isolated structural benchmark, whereas the fifth-order expansion provides a compact approximation with markedly improved accuracy.

The computational cost is not reported in terms of wall-clock time because such a quantity depends strongly on hardware, solver settings, sparse factorization details, and memory management. The number of degrees of freedom is therefore used only as a solver-independent proxy for computational size. In the coupled validation, LE16B3 reduces the total number of unknowns from 84,987 in the COMSOL reference model to 28,400, corresponding to approximately a factor of three in DoF count. This reduction suggests a potential computational advantage, especially for larger or multilayered configurations, for which the cross-sectional enrichment can be increased without uniformly refining the full three-dimensional mesh.

5 Results and discussion

This section examines the modal behavior predicted by the adopted high-order formulation by comparing *in vacuo* results with those from the fully coupled fluid–structure system. Attention is directed to modal correspondence between the *in vacuo* and coupled spectra and to the spectral modifications induced by fluid coupling. Particular emphasis is placed on how the adopted non-clamped edge conditions affect these trends and on the LE9B3 discretization's ability to reproduce the three-dimensional reference behavior at moderate computational cost.

For the simply-supported case, the single zero frequency corresponds to the residual rigid motion permitted by the adopted support idealization. The values in Table 6 should not be interpreted as a pure added-mass correction applied mode-by-mode to the uncoupled spectrum. Because the coupled problem contains hybrid structural-acoustic modes, the frequency shifts are discussed here only together with the MAC-based correspondence shown later in Fig. 4.

The data in Table 6 show that the coupled spectrum is shifted toward lower frequencies with respect to the *in*

Table 6 Comparison of eigenfrequencies between *in vacuo* (elastic) and coupled (fluid–structure) CUF LE9B3 models

	In vacuo	Coupled
Degrees of freedom	5859	46,221
Eigenfrequencies [Hz]	0	0
	1079	1079
	2408	2138
	3454	2139
	4231	2406
	6511	2681
	9224	2682
	9224	2915
	10,184	2916
	11,369	3333

Aluminum material, simply-supported structural, and pressure-release fluid boundary conditions

vacuo structural spectrum. This trend is consistent with the added inertia introduced by the surrounding fluid; however, the listed values should not be interpreted as one-to-one added-mass corrections for individual structural modes. The coupled eigenproblem contains hybrid structural-acoustic modes, and mode ordering can change when structural and acoustic resonances approach each other. For this reason, the frequency comparison is interpreted together with the MAC matrix in Fig. 4, which provides the relevant modal correspondence.

Particular attention should be paid to Fig. 2e. This coupled mode, located at 2138 Hz, reflects the hybridization between the structural deformation of the plate and the acoustic field in the surrounding cavity. The deformation pattern remains bending-dominated, but its correspondence with the *in vacuo* basis is established through the MAC analysis rather than through frequency ordering alone.

The data in Table 7 confirm that fluid coupling modifies the low-frequency spectrum; furthermore, the patterns displayed in Fig. 3 show that the principal bending character of each mode is preserved, albeit with a slight intensification of in-plane displacements in the vicinity of the free edges. In the free case, the first six zero-frequency modes correspond to the expected rigid-body modes of the unconstrained panel. Modal correspondence beyond these rigid-body modes is established through MAC and through inspection of the structural component of the coupled eigenvectors, rather than by frequency order alone, because repeated or closely spaced values occur around the first non-rigid modes.

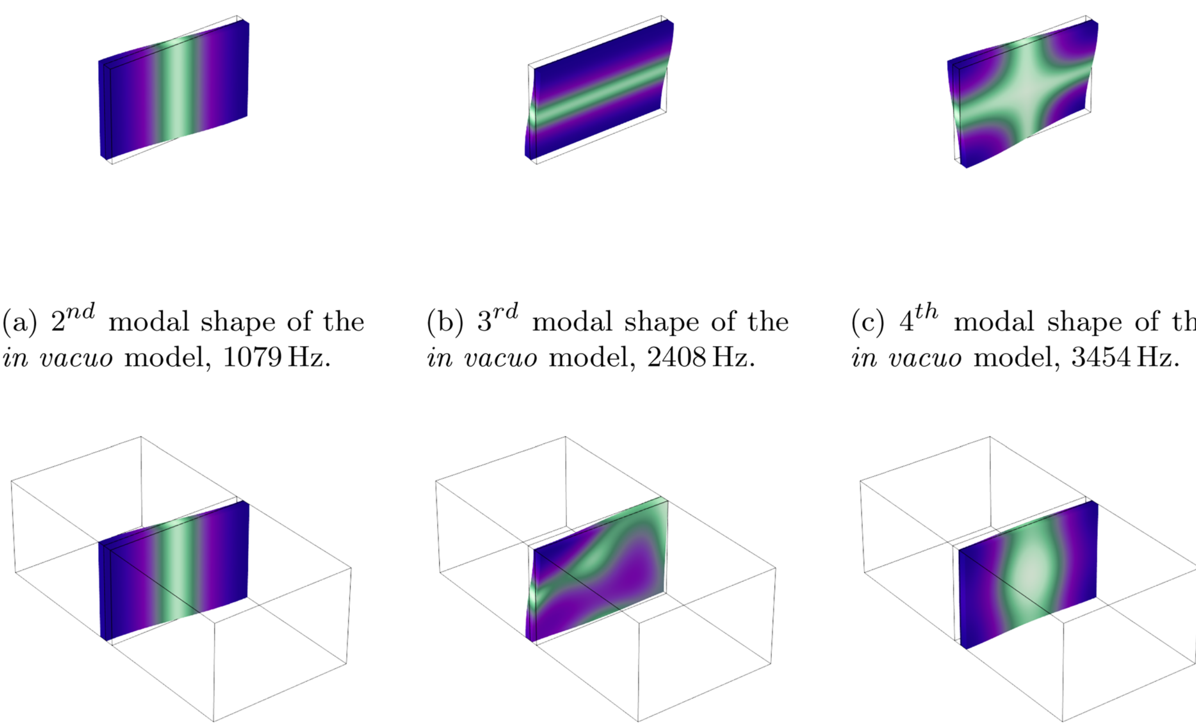

(a) 2^{nd} modal shape of the *in vacuo* model, 1079 Hz.
(b) 3^{rd} modal shape of the *in vacuo* model, 2408 Hz.
(c) 4^{th} modal shape of the *in vacuo* model, 3454 Hz.
(d) 2^{nd} modal shape of the coupled model, 1079 Hz.
(e) 3^{rd} modal shape of the coupled model, 2138 Hz.
(f) 4^{th} modal shape of the coupled model, 2139 Hz.

Fig. 2 Comparison of the first three non-rigid modal shapes between *in vacuo* (elastic) and coupled (fluid–structure) models. The structure's deformation is scaled to enhance visual comparison across all subfigures. Aluminum material, simply-supported structural, and pressure-release fluid boundary conditions

Table 7 Comparison of eigenfrequencies between *in vacuo* (elastic) and coupled (fluid–structure) CUF LE9B3 models

	In vacuo	Coupled
Degrees of freedom	5859	46,221
Eigenfrequencies [Hz]	0	0
	0	0
	0	0
	0	0
	0	0
	0	0
	2081	2079
	2298	2138
	4742	2140
	5300	2298

Aluminum material, free structural, and pressure-release fluid boundary conditions

Fluid coupling modifies the spectrum relative to the *in vacuo* condition through the combined action of fluid inertia, cavity compressibility, and modal hybridization; in the matched modes considered here, the dominant trend is a downward frequency shift. The MAC provides a quantitative overview of this correspondence, computed between the structural and coupled eigenvectors and visualized in Fig. 4. For this reason, generalized added-mass values are not introduced as primary descriptors in the present paper: the comparison is carried out in terms of coupled modal correspondence rather than through projection onto a fixed uncoupled structural basis.

Overall, the numerical evidence supports the consistency and computational compactness of the CUF-based approach within the benchmark cases considered. The adoption of high-order cross-sectional expansions reduces the number of DoFs required to obtain converged numerical solutions, thereby offering a compact alternative to full three-dimensional discretizations.

6 Conclusions and outlook

The present study has extended and assessed the previously developed CUF-based coupled vibroacoustic modal framework for rectangular plates under simply-supported and free edge conditions. Comparison with three-dimensional FE benchmarks showed sub-percent frequency discrepancies for the Lagrange hierarchy in the considered coupled configurations. The Taylor hierarchy showed the expected

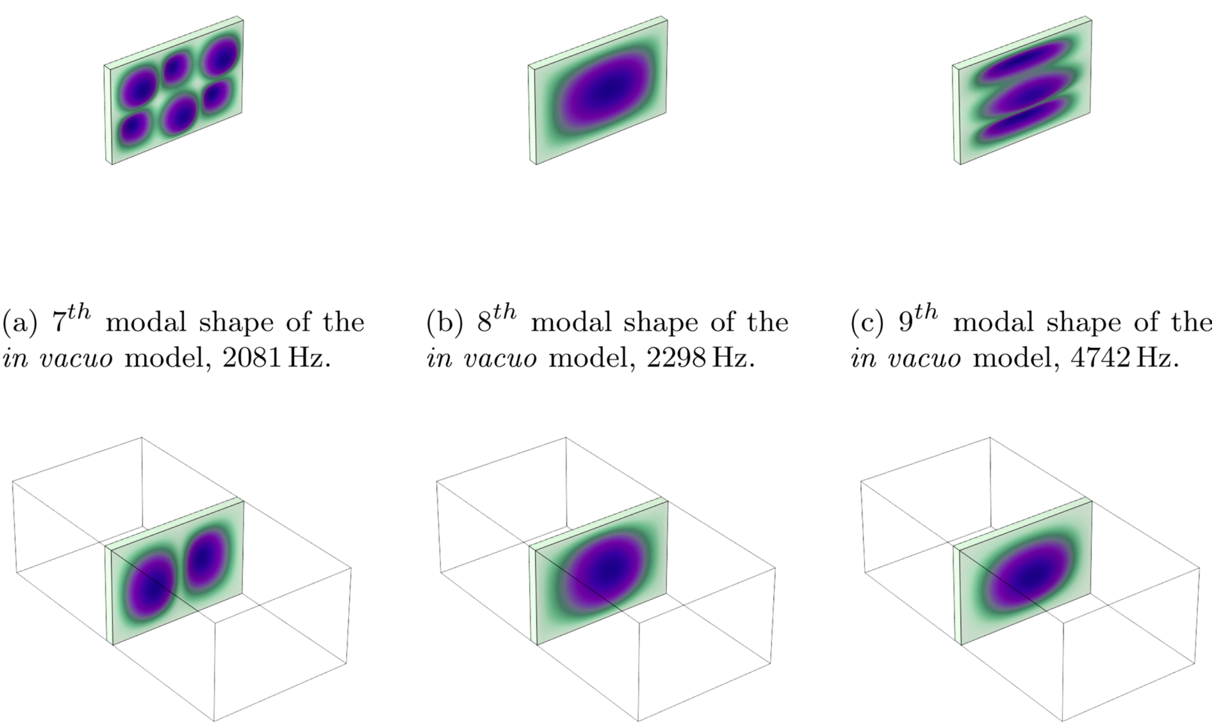

(a) 7^{th} modal shape of the *in vacuo* model, 2081 Hz. (b) 8^{th} modal shape of the *in vacuo* model, 2298 Hz. (c) 9^{th} modal shape of the *in vacuo* model, 4742 Hz.

(d) 7^{th} modal shape of the coupled model, 2079 Hz. (e) 8^{th} modal shape of the coupled model, 2138 Hz. (f) 9^{th} modal shape of the coupled model, 2140 Hz.

Fig. 3 Comparison of the first three non-rigid modal shapes between *in vacuo* (elastic) and coupled (fluid–structure) models. The structure's deformation is scaled to enhance visual comparison across all subfigures. Aluminum material, free structural, and pressure-release fluid boundary conditions

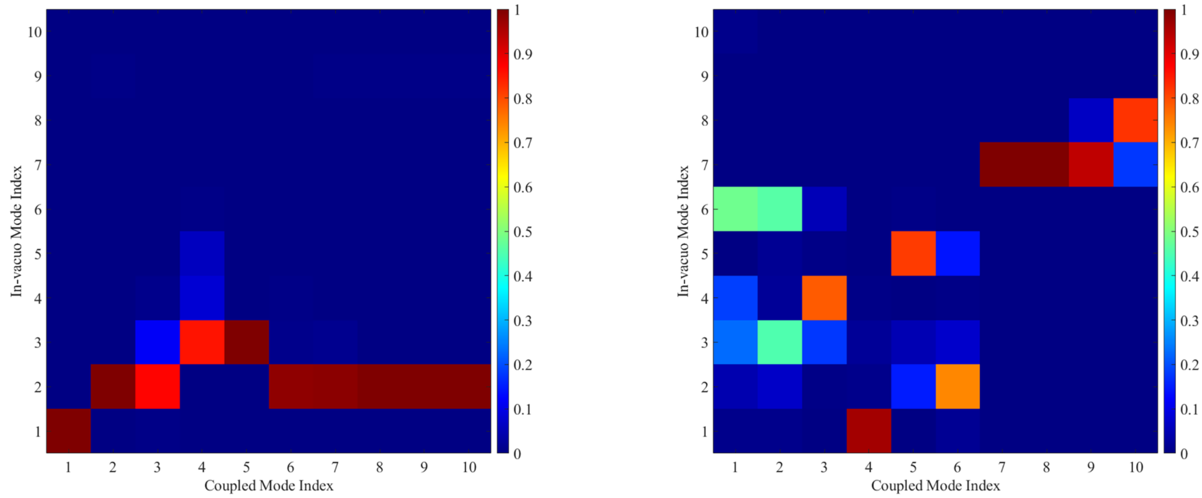

(a) Aluminum material, simply-supported structural and pressure-release fluid boundary conditions.

(b) Aluminum material, free structural and pressure-release fluid boundary conditions.

Fig. 4 MAC between *in vacuo* (elastic) and coupled (fluid–structure) CUF LE9B3 models

convergence with increasing truncation order, although the lower-order Taylor models were not uniformly accurate for the isolated structural benchmark. The MAC-based comparisons indicated that the structural component of the coupled eigenvectors can be tracked against the *in vacuo* solutions, while the spectrum is modified by fluid inertia, cavity compressibility, and modal hybridization.

Compared with the previously studied clamped case, relaxing the edge constraints to the present simply-supported and free configurations produces lower natural frequencies and more pronounced in-plane activity near the boundaries, especially once the structural and acoustic wavelengths become comparable.

It should be emphasized that the present contribution is deliberately positioned within computational mechanics: the investigated configurations are controlled numerical benchmarks for testing the CUF-based coupled formulation, rather than application-specific designs requiring direct experimental validation on a dedicated rig, which is left to future work. At present, reliability is supported by mesh convergence, comparison with an independent three-dimensional FE implementation, MAC-based modal tracking, and analytical verification of the isolated rigid-fluid cavity. The analytical check applies only to the isolated acoustic subproblem, whereas the coupled plate-fluid system is verified numerically. Moreover, the analysis is restricted to small-amplitude linear elasticity and inviscid linear acoustics. Damping, manufacturing tolerances, fixture compliance, exterior-radiation effects, and measurement uncertainty are not included in the present study.

Future developments may focus on extending the present framework to (i) geometrically nonlinear kinematics to capture amplitude-dependent modal interaction, (ii) frequency-dependent viscoelastic damping layers and locally reactive acoustic liners, and (iii) transient analyses driven by broadband excitation, which will enable time-resolved validation against experimental measurements. Another interesting research direction is to integrate gradient-based sensitivity analysis into the CUF hierarchy, paving the way for the design optimization of fluid-loaded structures under stringent weight and noise constraints.

Acknowledgements The authors acknowledge the support of the Italian Ministry of University and Research (MUR) and the Sustainable Mobility Center (MOST) through the project PNRR-M4C2-CNMS-Spoke 1, funded under the scheme CN00000023-PNRR-M4C2 Inv. 1.4 (grant no. 55-PRR22-1155-22-GG002138).

Author contributions D.M.: Conceptualization; Formal analysis; Investigation; Methodology; Validation; Writing—original draft; Writing—review & editing.

Funding Open access funding provided by Politecnico di Torino within the CRUI-CARE Agreement.

Data availability No datasets were generated or analysed during the current study.

Declarations

Competing interest The authors declare no competing interest.

References

1. Paidoussis, M.P.: Fluid-structure interactions: slender structures and axial flow (2nd edn), vol. 2, Academic Press, Oxford (2014)
2. Giunta, G., Carrera, E.: Component-wise analysis of laminated anisotropic composites. Int. J. Solids Struct. **49**(13), 1839–1851 (2012). https://doi.org/10.1016/j.ijsolstr.2012.03.025
3. Moruzzi, M.C., Cinefra, M., Bagassi, S., Zappino, E.: Vibroacoustic analysis of composite plate-cavity systems via CUF finite elements. Compos. Struct. **259**, 113428 (2021). https://doi.org/10.1016/j.compstruct.2020.113428
4. Biedermann, J., Winter, R., Wandel, M., Böswald, M.: Energy based correlation criteria in the mid-frequency range. J. Sound Vib. **400**, 457–480 (2017). https://doi.org/10.1016/j.jsv.2017.04.024
5. Casaburo, A., Magliacano, D., Petrone, G., Franco, F., De Rosa, S.: Optimizing the acoustic properties of a meta-material using machine learning techniques, pp. 1948–1959. Washington, USA (2021)
6. Tavares, A., Di Lorenzo, E., Cornelis, B.: Automated experimental modal analysis with density-based clustering: a benchmark validation through jury testing. Mech. Syst. Signal Process. **232**, 112714 (2025). https://doi.org/10.1016/j.ymssp.2025.112714
7. Amabili, M., Paidoussis, M.P.: Review of studies on geometrically nonlinear vibrations and dynamics of circular cylindrical shells and panels, with and without fluid-structure interaction. Appl. Mech. Rev. **56**(4), 349–381 (2003). https://doi.org/10.1115/1.1565084
8. Magliacano, D., Ouisse, M., Khelif, A., De Rosa, S., Franco, F., Atalla, N.: Computation of wave dispersion characteristics in periodic porous materials modeled as equivalent fluids, pp. 4741–4751. Leuven, Belgium (2018)
9. Catapane, G., Magliacano, D., Petrone, G., Casaburo, A., Franco, F., De Rosa, S.: Labyrinth resonator design for low-frequency acoustic meta-structures. Mechanisms and Machine Science 125 MMS, pp. 681–694 (2022) https://doi.org/10.1007/978-3-031-15758-5_70
10. Nguyen, N.D.: A new higher-order beam theory for buckling and free vibration responses of laminated composite and functionally graded porous beams. J. Strain Anal. Eng. Des. **59**(1), 67–81 (2023). https://doi.org/10.1177/03093247231187454
11. Carrera, E., Zappino, E.: Carrera unified formulation for free-vibration analysis of aircraft structures. AIAA J. **54**(1), 280–292 (2016). https://doi.org/10.2514/1.J054265
12. Pagani, A., Carrera, E.: Unified formulation of geometrically nonlinear refined beam theories. Mech. Adv. Mater. Struct. **25**(1), 15–31 (2018). https://doi.org/10.1080/15376494.2016.1232458
13. Petrolo, M., Kaleel, I., De Pietro, G., Carrera, E.: Wave propagation in compact, thin-walled, layered, and heterogeneous structures using variable kinematics finite elements. Int. J. Comput. Methods Eng. Sci. Mech. **19**(3), 207–220 (2018). https://doi.org/10.1080/15502287.2018.1447048
14. Davis, R.B.: Techniques to assess acoustic–structure interaction in liquid rocket engines. PhD thesis, Duke University, Durham, NC, USA (2008)
15. Magliacano, D.: High-order vibroacoustic modal analysis framework for fluid-structure coupling. Aerospace **12**(11), 994 (2025). https://doi.org/10.3390/aerospace12110994
16. Allemang, R.J.: The modal assurance criterion—twenty years of use and abuse. In: Proc. IMAC XXI, Kissimmee, FL (2003)
17. Zhang, J., Jiao, R.: Vibro-acoustic modeling of a rectangular enclosure with a flexible panel in a broad frequency range and experimental investigations. J Vibroeng **18**(4), 2683–2692 (2016)
18. Everstine, G.C.: A symmetric potential formulation for fluid–structure interaction. J. Sound Vib. **79**(1), 157–160 (1981). https://doi.org/10.1016/0022-460X(81)90335-7
19. Wang, X., Bathe, K.-J.: Displacement/pressure based mixed finite element formulations for acoustic fluid-structure interaction problems. Int. J. Numer. Meth. Eng. **40**(11), 2001–2017 (1997).
20. Ihlenburg, F.: Finite element analysis of acoustic scattering. Springer, New York (1998)
21. Atalla, N., Sgard, F.: Finite element and boundary methods in structural acoustics and vibration, 1st edn. CRC Press, Boca Raton, FL (2015)
22. Marburg, S., Nolte, B. (eds.): Computational acoustics of noise propagation in fluids: finite and boundary element methods. Springer, Berlin, Heidelberg (2008)
23. Moukhliss, A., Rahmouni, A., Bouksour, O., Benamar, R.: Using the discrete model for the processing of natural vibrations, tapered beams made of afg materials carrying masses at different spots. Mater Today: Proc **52**, 21–28 (2022). https://doi.org/10.1016/j.matpr.2021.10.107
24. Moukhliss, A., Ayoub, N., Rahmouni, A., Benamar, R.: Advanced crack detection in bidirectional gradient material fgm beams: a neural network approach with adam optimization. Iran. J. Sci. Technol. Trans. Mech. Eng. **49**(2), 963–988 (2025). https://doi.org/10.1007/s40997-024-00813-7
25. Moukhliss, A., Rahmouni, A., Benamar, R.: A discrete model for analyzing the free vibrations of a non-uniform 2d-fgm beam under elastic foundations and different support conditions. Sci. Rep. **16**, 2458 (2026). https://doi.org/10.1038/s41598-025-32206-4
26. Huang, J., Xu, W., Zhou, H.: Free vibration analysis of exponentially non-uniform beams with tip mass. J. Braz. Soc. Mech. Sci. Eng. **47**(12), 633 (2025)
27. Özdemir, O.: Vibration and buckling analyses of rotating axially functionally graded nonuniform beams. J. Vib. Eng. Technol. **10**(4), 1381–1397 (2022). https://doi.org/10.1007/s42417-022-00453-8
28. Cinefra, M., Kumar, S.K., Carrera, E.: MITC9 shell elements based on RMVT and CUF for the analysis of laminated composite plates and shells. Compos. Struct. **209**, 383–390 (2019). https://doi.org/10.1016/j.compstruct.2018.10.039
29. Arruda, M.R.T., Castro, L.M.S., Ferreira, A.J.M.: Analysis of composite layered beams using Carrera unified formulation with Legendre approximation. Compos. B Eng. **137**, 23–40 (2017). https://doi.org/10.1016/j.compositesb.2017.10.040
30. Carrera, E., Pagani, A., Augello, R.: On the role of large cross-sectional deformations in the nonlinear analysis of composite thin-walled structures. Arch. Appl. Mech. **91**, 1605–1621 (2021). https://doi.org/10.1007/s00419-020-01843-8
31. Magliacano, D., Tufano, V., Letizia, A., Sessa, B., Filippi, M.: Data-driven failure criteria prediction in composite wing boxes using machine learning. Compos. Struct. (2025). https://doi.org/10.1016/j.compstruct.2025.119675
32. Magliacano, D., Letizia, A., Di Palo, S., Alecci, M., Bazzani, M.: Element-level finite-element-informed machine-learning surrogates for failure-index prediction in a composite wing box with

intralaminar damage. Aerosp. Sci. Technol. **177**, 112878 (2026). https://doi.org/10.1016/j.ast.2026.112878
33. Moruzzi, M.C., Cinefra, M., Bagassi, S.: Analysis of an acoustic monopole source in a closed cavity via CUF finite elements. Aerotec Missili Spaz **101**, 371–385 (2022). https://doi.org/10.1007/s42496-022-00129-2
34. Roache, P.J.: Verification and validation in computational science and engineering. Hermosa Publishers, Albuquerque, NM (1998)
35. ASME V&V 10-2006: Guide for verification and validation in computational solid mechanics. American Society of Mechanical Engineers (2006)
36. Magliacano, D., Ouisse, M., De Rosa, S., Franco, F., Khelif, A.: Investigations about the modelling of acoustic properties of periodic porous materials with the shift cell approach. In: 9th ECCOMAS Thematic Conference on Smart Structures and Materials, pp. 1112–1123. SMART, Paris, France (2019)
37. Kinsler, L.E., Frey, A.R., Coppens, A.B., Sanders, J.V.: Fundamentals of acoustics, 4th edn. Wiley, New York (2000)